ChemSusChem

Supporting Information

First-Principles Studies on the Atomistic Properties of Metallic Magnesium as Anode Material in Magnesium-Ion Batteries

Florian Fiesinger, Daniel Gaissmaier, Matthias van den Borg, and Timo Jacob*

Table of Contents

Theoretical section

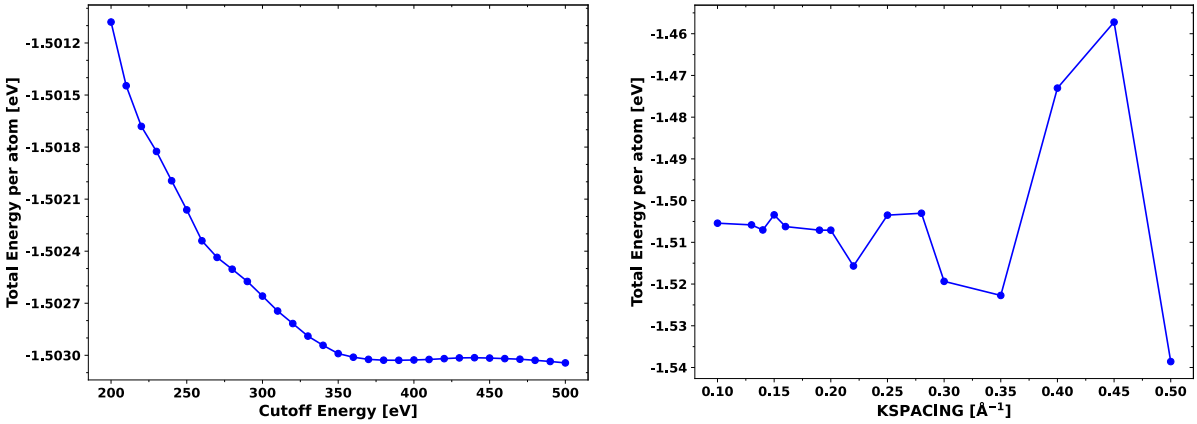

Figure S1. Convergence studies of the cutoff energy (≙ ENCUT Tag) and grid density of the k-points (≙ KSPACING Tag).

Table S1. Number of layers used for the calculation of surface energies.

Surface	Layers	Surface	Layers
Mg(0001)	7	Mg(11$\bar{2}$2)	24
Mg(10$\bar{1}$0)A/ Mg(10$\bar{1}$0)B	12	Mg(11$\bar{2}$0)	20
Mg(10$\bar{1}$1)	14	Mg(21$\bar{3}$1)	32
Mg(10$\bar{1}$2)A/ Mg(10$\bar{1}$2)B	18	Mg(22$\bar{4}$1)	40
Mg(21$\bar{3}$0)A/ Mg(21$\bar{3}$0)B	30	Mg(11$\bar{2}$1)	22
Mg(21$\bar{3}$2)	32	Mg(20$\bar{2}$1)	24

Table S2. Surface directions, number of layers and supercell used for the calculation of adsorption, dimer interaction, diffusion, and frequency properties. One layer consists of 2 Mg atoms for Mg(0001). The asterisk * indicates the use of vicinal slabs.

Surface	Property/Process	Direction	Layers	Supercell
Mg(0001)	Adsorption, Dimer interaction	[0001]	3	6×6
	Terrace, Dimer, Trimer			
	Kink, Inner-corner, Outer-corner ([$\bar{1}\bar{1}$20]-step)	[10$\bar{1}$6]*	20	6×1
	Kink, Inner-corner, Outer-corner ([11$\bar{2}$0]-step)	[10$\bar{1}\bar{6}$]*	20	6×1
	Step-edge, Step-vacancy, Step-down, Step-down (dimer), Upper-step ([$\bar{1}\bar{1}$20]-step)	[10$\bar{1}$8]*	26	4×1
	Step-edge, Step-vacancy, Step-down, Step-down (dimer), Upper-step ([11$\bar{2}$0]-step)	[10$\bar{1}\bar{8}$]*	26	4×1
Mg(10$\bar{1}$0)	Adsorption, Dimer interaction	[10$\bar{1}$0]	6	6×3
	Terrace			
Mg(10$\bar{1}$1)	Adsorption, Dimer interaction	[10$\bar{1}$1]	6	6×3
	Terrace, Dimer, Trimer			
	Step-edge, Step-down ([$\bar{1}$2$\bar{1}$0]A/B-step)	[30$\bar{3}$2]*	18	5×1
	Step-edge, Step-down ([1$\bar{2}$10]A/B-step)	[30$\bar{3}$4]*	21	5×1
	Step-edge, Step-down ([10$\bar{1}$2]-step)	[51$\bar{6}$5]*	34	3×1

Bulk properties

The bulk properties of magnesium, including lattice constants, binding energies, and bulk moduli, were calculated for the following crystal structures with the PBE and the BEEF-vdW functional: hexagonal-closed-packed (*hcp*), double-hexagonal-closed-packed (*dhcp*), body-centered-cubic (*bcc*), face-centered-cubic (*fcc*), simple cubic (*sc*), β-tungsten (*a15*) and diamond (*dia*). The calculated values for both functionals for all crystal structures and a comparison with experimentally obtained data are shown in Table S3. Magnesium crystallizes in accordance with experimental studies in a *hcp* structure under ambient conditions. The calculated cohesive energy of 1.50 eV·atom^{-1} (Equation (S1)) from the PBE functional is in almost perfect agreement with the experimental value (Table S3) and with other theoretical studies (Table S4). The BEEF-vdW functional slightly underestimates the cohesive energy, but it is within its estimated error. Moriarty *et al.* first predicted a phase transformation from the *hcp* to the *bcc* structure at around 50 GPa from generalized pseudopotential theory[1–3], which Olijnyk and Holzapfel later confirmed by X-ray diffraction (XRD).[4] This is contradicted by the study of Erandonea *et al.*, who assumed the *dhcp* instead of the *bcc* structure at high pressures and temperatures.[5] Moriarty *et al.* also predicted a second phase transformation from the *bcc* to the *fcc* structure at even higher pressures[2], which could not be observed experimentally.[6]

Table S3. Calculated and experimentally observed physical constants for different bulk phases of magnesium. The lattice constants a_0 and c_0 are given in Å, bulk moduli B_0 in GPa, and the cohesive energy E_{coh} (Equation (S1)) in eV·atom^{-1}. For the BEEF-vdW functional, the calculated standard deviation of the cohesive energy is given in parenthesis. The experimental results were taken from Kittel *et al.*[7] The influence of the zero-point vibrational energy E_{ZPVE} on the experimental values is given in parentheses. The values were adapted from Alchagirov *et al.* for a_0, c_0, and B_0 and calculated with Equation (S2) for E_{coh}.[8]

Bulk properties		This work		Other works
		PBE	BEEF-vdW	Experiment
hcp	a_0	3.18	3.19	3.21 (0.00)
	c_0	5.21	5.21	5.21 (0.00)
	B_0	36.5	37.1	35.4 (-0.04)
	E_{coh}	1.50	1.33 (0.27)	1.51 (0.04)
dhcp	a_0	3.19	3.18	
	c_0	10.43	10.43	
	B_0	36.1	36.7	
	E_{coh}	1.49	1.33	
bcc	a_0	3.57	3.58	
	B_0	35.3	35.4	
	E_{coh}	1.48	1.30 (0.28)	
fcc	a_0	4.52	4.52	
	B_0	35.9	36.66	
	E_{coh}	1.49	1.32 (0.27)	
sc	a_0	3.02	3.02	
	B_0	23.2	23.2	
	E_{coh}	1.12	0.94 (0.22)	
a15	a_0	5.72	5.72	
	B_0	34.7	35.1	

	E_{coh}	1.46	1.28 (0.27)	
dia	a_0	6.85	6.97	
	B_0	10.9	9.1	
	E_{coh}	0.73	0.56 (0.11)	

Table S4. Calculated (PBE/BEEF-vdW) and literature physical constants of the *hcp* bulk phase of magnesium. The lattice constants a_0 and c_0 are given in Å, bulk moduli B_0 in GPa and the cohesive energy E_{coh} in eV·atom^{-1}.

Bulk properties		a_0	c_0	B_0	E_{coh}	Code
This work	**PBE**	3.18	5.21	36.5	1.50	VASP
	BEEF-vdW	3.19	5.21	37.1	1.33	VASP
Other works	**PBE**[9]	3.19	5.18	-	1.51	VASP
	PBE[10]	3.19	5.18	-	1.50	VASP
	PBE[11]	3.22	5.12	-	1.50	VASP
	PW91[12]	3.21	5.16	35.5	1.45	Quantum Espresso
	PBE[12]	3.20	5.20	-	1.50	VASP
	PW91[13]	3.18	5.14	35.5	1.50	fhi96md
	PBE[14]	3.19	5.18	-	-	VASP
	LDA[14]	3.12	5.08	-	-	VASP
	PBE[15]	3.19	5.22	-	-	VASP
	PW91[15]	3.19	5.20	-	-	VASP
	PBE[16]	3.19	5.18	-	-	VASP
	Experiment[7]	3.21	5.21	35.6	1.51	

The cohesive energy E_{coh} is defined as the energy gain an isolated atom receives when it is embedded in a certain crystal structure. It was calculated by subtracting the energies of the isolated atoms E_{atom} from the energy of the bulk crystal structure E_{bulk}, divided by the total number of atoms N in the bulk structure:

$$E_{\mathrm{coh}} = -\frac{1}{N}(E_{\mathrm{bulk}} - N \cdot E_{\mathrm{atom}}) \quad \text{(S1)}$$

Bulk moduli were calculated based on the jellium equation of state.[17] In order to be able to compare the theoretical cohesive energy with the experimental reference, the zero-point vibrational energy E_{ZPVE} was estimated as follows:[8]

$$E_{\mathrm{ZPVE}} = \frac{9}{8} k_{\mathrm{B}} \theta_{\mathrm{D}} \quad \text{(S2)}$$

k_{B} corresponds to the Boltzmann constant and θ_{D} to the Debye temperature, which is 400 K for magnesium.[8]

Surface properties

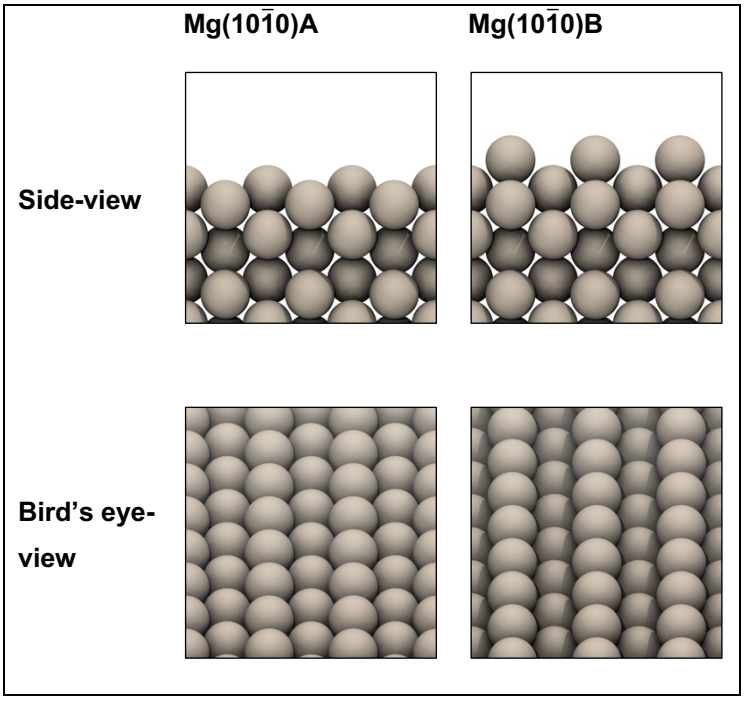

Figure S2. Representation of the surface terminations A and B of surface Mg(10$\bar{1}$0). The respective structures are shown in a side- and a bird's eye-view.

Table S5. Calculated (PBE/BEEF-vdW) and literature surface energies γ for low- and high-index surfaces of magnesium. The surface energy γ is given in meV·Å^{-2}. For the BEEF-vdW functional the calculated standard deviation of the surface energy is given in parenthesis.

γ	This work		Other works			
	PBE	BEEF-vdW	PBE	PBEsol	EAM	Experiment
Mg(0001)	33.9	38.7 (9)	34.6[9], 32.5[10], 32.5[11], 33.0[14], 31.8[18]	39.0[15], 35.0[16]	31.0[19]	51.0[20]
Mg(10$\bar{1}$0)A	40.2	44.9 (9)	39.9[9], 40.1[14], 37.4[18]		32.0[19]	
Mg(10$\bar{1}$1)	40.9	45.8 (8)	40.9[9], 46.4[14], 39.3[18]	45.9[15], 51.2[16]	31.1[19]	
Mg(10$\bar{1}$2)A	44.9	49.6 (10)	38.4[14], 43.7[18]			
Mg(21$\bar{3}$0)A	45.9	50.6 (10)	46.6[14], 43.7[18]			
Mg(10$\bar{1}$2)B	46.1	50.9 (10)				
Mg(21$\bar{3}$2)	46.7	51.3 (10)	46.2[18]			
Mg(11$\bar{2}$2)	46.8	51.3 (10)	48.4[14], 46.2[18]			
Mg(11$\bar{2}$0)	47.1	51.7 (10)	45.7[9], 44.9[18]	51.4[15], 34.3[16]		
Mg(21$\bar{3}$1)	47.1	51.7 (10)	45.6[18]			
Mg(22$\bar{4}$1)	47.9	52.5 (10)	46.8[18]			
Mg(11$\bar{2}$1)	48.7	53.0 (10)	48.1[9], 47.7[14], 47.4[18]			
Mg(20$\bar{2}$1)	48.8	53.4 (10)	48.1[18]			
Mg(21$\bar{3}$0)B	52.0	56.3 (11)		56.1[15]		
Mg(10$\bar{1}$0)B	55.5	59.4 (11)	53.7[11]	60.6[15], 38.5[16]		

Adsorption properties

The adsorption energy provides information about which positions are preferentially populated. Consequently, adsorption of Mg was studied on the surfaces present according to the Wulff shape (Mg(0001), Mg(10$\bar{1}$0)A, Mg(10$\bar{1}$1)) as well as, for the sake of completeness, on Mg(10$\bar{1}$0)B. The respective adsorption energies (PBE/BEEF-vdW) and available literature data (PBE) are summarized in Table S6. In addition, a schematic representation of all adsorption sites studied is provided in Figure S3.

The highest energy gain results from adsorption on the *bridge-bottom* position on Mg(10$\bar{1}$0)B (-1.64 eV), which is also the only stable adsorption site on this surface. The high adsorption energy seems logical since Mg(10$\bar{1}$0)B, the surface termination with the highest surface energy, aims for its stabilization by a transformation into the much more stable counterpart Mg(10$\bar{1}$0)A. In fact, this becomes even more evident when comparing the structural environments of the adsorption sites in Figure S3. Mg(10$\bar{1}$0)B is characterized by deep channels running parallel. Adsorption at the *bridge-bottom* position coordinates the adsorbate to six adjacent neighbors, more than in any other site, regardless of the surface. The second highest adsorption energy was found for Mg(10$\bar{1}$0)A at the *ontop-bottom* site (-1.00 eV), significantly lower than on Mg(10$\bar{1}$0)B. Mg(10$\bar{1}$0)A also exhibits channels, although they are not as deep as in Mg(10$\bar{1}$0)B, and the number of coordination partners of an adsorbate is reduced to five. Following closely behind with a 0.03 eV lower adsorption energy (-0.97 eV) is the *hollow* site on Mg(10$\bar{1}$1), where the adsorbate has a coordination number of four. These two sites have the highest adsorption energies for the surfaces present in the Wulff shape, indicating primary adsorption to occur on Mg(10$\bar{1}$0)A and Mg(10$\bar{1}$1).

There are two stable adsorption sites in the case of the most stable surface Mg(0001). Preferred adsorption occurs at the *fcc* site (-0.58 eV), which is energetically slightly favored compared to the *hcp* site (-0.56 eV). Thus, both adsorption energies are approximately 40% lower than the corresponding adsorption energies on Mg(10$\bar{1}$0)A and Mg(10$\bar{1}$1). Clarification may be found again by considering the morphology. Mg(0001) has a flat surface with a high packaging density. The coordination of the adsorbate occurs only to three surface atoms. Moreover, the energetically similar but unstable *bridge* site already allows the prediction of a low terrace self-diffusion barrier. At this point, we refer to the work of Lautar *et al.* in which potential energy surfaces (PES) were calculated, clearly showing the varying energy landscapes for Mg(0001), Mg(10$\bar{1}$0)A, and Mg(10$\bar{1}$1).[9] We also want to reference two EAM potentials for magnesium by Liu et *al*.[21] and Sun et *al*.[22] However, in the potential of Liu et *al*., only the *bridge* position on Mg(0001) is stable, which is not the case according to our DFT calculations.[19] We also want to point to the section Dimer and trimer self-diffusion on Mg(0001) and Mg(10$\bar{1}$1), which further clarifies why *fcc* sites are energetically favored over hcp sites, although this contradicts the nature of the *hcp* lattice, which should follow the ABABAB-stacking sequence.

All calculated adsorption energies are consistent with previously published theoretical results (on PBE level).[9,10,12,23] The error range for the BEEF-vdW functional varies between 0.10 and 0.31 eV, indicating a strong dependence on the chosen functional. However, all PBE results are within the BEEF-vdW standard deviation, and the energy ratios are equal for both functionals.

Table S6. The adsorption energies E_{ad} of an adsorbed Mg atom on Mg(0001), Mg(10$\bar{1}$0) and Mg(10$\bar{1}$1) calculated with Equation (S3) (PBE and BEEF-vdW) and literature data. All values are given in eV·atom^{-1}. For the BEEF-vdW functional, the calculated standard deviation of the adsorption energy E_{ad} is given in parenthesis. A schematic representation of all adsorption sites studied is given in Figure S3.

E_{ad}	Adsorption site	This work		Other works
		PBE	BEEF-vdW	PBE
Mg(0001)	fcc	-0.58	-0.48 (0.15)	-0.58[9], -0.59[10]
	hcp	-0.56	-0.47 (0.14)	-0.56[9], -0.57[10]
	bridge[a]	-0.56	-0.46 (0.14)	-0.57[10]
	ontop[a]	-0.45	-0.38 (0.12)	-0.44[10]
Mg(10$\bar{1}$0)A	ontop-bottom	-1.00	-0.86 (0.23)	-1.03[9]
	bridge-bottom[a]	-0.97	-0.84 (0.21)	
	ontop-up[a]	-0.46	-0.42 (0.10)	
	bridge-up[a]	-0.58	-0.51 (0.12)	
Mg(10$\bar{1}$0)B	ontop-bottom[a]	-1.23	-1.04 (0.25)	
	bridge-bottom	-1.64	-1.45 (0.31)	
	ontop-up[a]	-0.42	-0.38 (0.10)	
	bridge-up[a]	-0.52	-0.50 (0.12)	
Mg(10$\bar{1}$1)	hollow	-0.97	-0.83 (0.19)	-0.97[9]

[a] unstable configuration; fixed with constraints.

Adsorption energies E_{ad} were obtained by subtracting the energy of the pure surface E_{slab} plus the energy of an isolated magnesium atom $E_{\mathrm{Mg-atom}}$ from the energy of the relaxed system E_{tot} containing the slab with the adsorbed atom:

$$E_{\mathrm{ad}} = E_{\mathrm{tot}} - (E_{\mathrm{slab}} + E_{\mathrm{Mg-atom}}) \quad \text{(S3)}$$

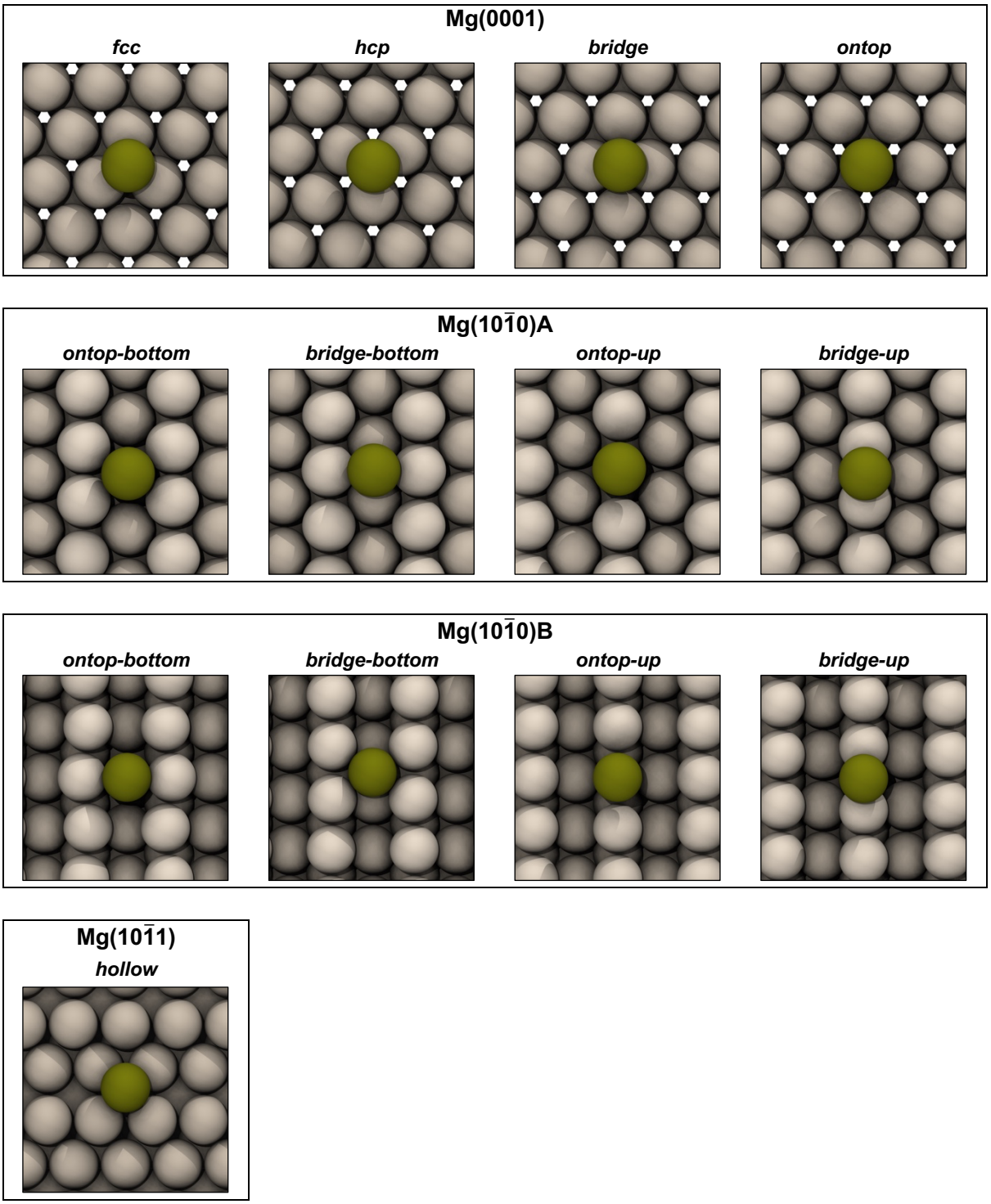

Figure S3. Schematic representation of the adsorption sites on Mg(0001), on the two surface terminations A and B of Mg(10$\bar{1}$0) and on Mg(10$\bar{1}$1).

Diffusion properties

Table S7. Pre-exponential factors ν, activation energies E_a, rate constants $k_{@RT}$, and activation temperatures T_a for forward and backward terrace self-diffusion processes from PBE calculations. The values are given in 10^{12} Hertz, eV, Hz, and K, respectively.

Terrace	Pathway	ν^{for}	E_a^{for}	$k_{@RT}^{for}$	T_a^{for}	ν^{rev}	E_a^{rev}	$k_{@RT}^{rev}$	T_a^{rev}
Mg(0001)	$fcc_0 \leftrightarrow hcp_1$	0.6	0.02	2.7E+11	9	1.3	0.01	1.0E+12	2
	$fcc_0 \leftrightarrow hcp_2$ (Ex.)	3.0	0.74	6.0E-01	298	4.1	0.72	1.6E+00	289
Mg(10$\bar{1}$0)	$ob_0 \leftrightarrow ob_1$	1.2	0.02	4.6E+11	10	1.2	0.02	4.6E+11	10
	$ob_0 \leftrightarrow ob_2$	1.2	0.42	6.8E+04	176	1.2	0.42	6.8E+04	176
	$ob_0 \leftrightarrow ob_2$ (Ex.)	0.7	0.46	7.3E+03	198	0.7	0.46	7.3E+03	198
Mg(10$\bar{1}$1)	$h_0 \leftrightarrow h_1$	7.2	0.30	5.2E+07	117	7.2	0.30	5.2E+07	117
	$h_0 \leftrightarrow h_1$ (Ex.)	4.7	0.59	3.0E+02	236	4.7	0.59	3.0E+02	236
	$h_0 \leftrightarrow h_2$	4.5	0.42	2.5E+05	168	7.8	0.42	4.3E+05	165

Table S8. Pre-exponential factors ν, activation energies E_a, rate constants $k_{@RT}$, and activation temperatures T_a for forward and backward terrace self-diffusion processes from BEEF-vdW calculations. The values are given in 10^{12} Hertz, eV, Hz, and K, respectively.

Terrace	Pathway	ν^{for}	E_a^{for}	$k_{@RT}^{for}$	T_a^{for}	ν^{rev}	E_a^{rev}	$k_{@RT}^{rev}$	T_a^{rev}
Mg(0001)	$fcc_0 \leftrightarrow hcp_1$	3.5	0.02 (0.02)	1.5E+12	8	3.4	0.01 (0.01)	2.6E+12	4
	$fcc_0 \leftrightarrow hcp_2$ (Ex.)	5.8	0.79 (0.23)	1.7E-01	312	9.6	0.77 (0.23)	5.3E-01	299
Mg(10$\bar{1}$0)	$ob_0 \leftrightarrow ob_1$	8.1	0.02 (0.04)	3.8E+12	8	8.1	0.02 (0.04)	3.8E+12	8
	$ob_0 \leftrightarrow ob_2$	6.2	0.35 (0.15)	6.7E+06	138	6.2	0.35 (0.15)	6.7E+06	138
	$ob_0 \leftrightarrow ob_2$ (Ex.)	4.8	0.47 (0.14)	3.7E+04	187	4.8	0.47 (0.14)	3.7E+04	187
Mg(10$\bar{1}$1)	$h_0 \leftrightarrow h_1$	5.8	0.27 (0.06)	1.2E+08	107	5.8	0.27 (0.06)	1.2E+08	107
	$h_0 \leftrightarrow h_1$ (Ex.)	1.7	0.62 (0.16)	3.4E+01	255	1.7	0.62 (0.16)	3.4E+01	255
	$h_0 \leftrightarrow h_2$	5.4	0.38 (0.08)	1.8E+06	150	4.7	0.38 (0.08)	1.6E+06	151

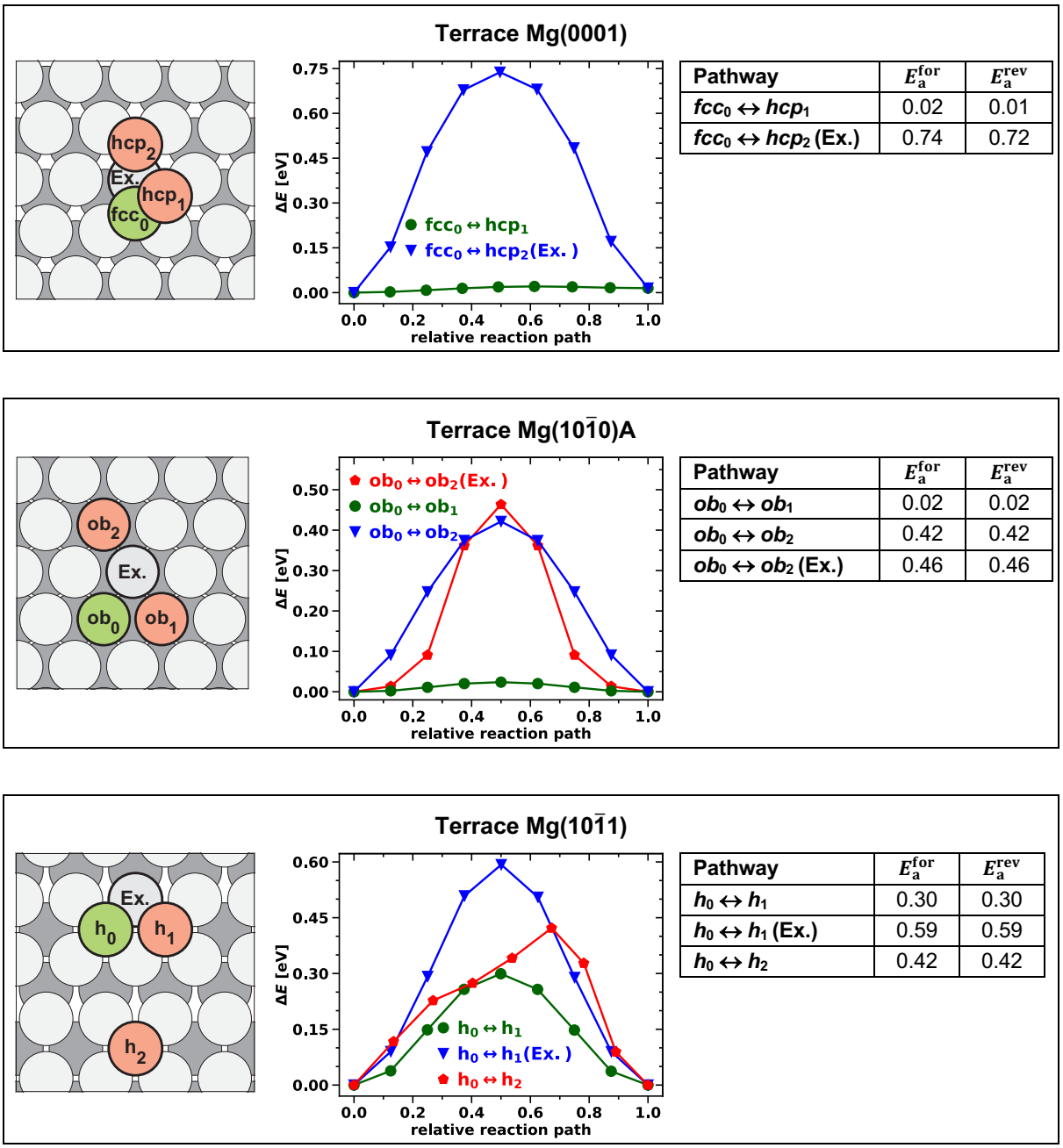

Pathway	E_a^{for}	E_a^{rev}
fcc$_0$ ↔ *hcp*$_1$	0.02	0.01
fcc$_0$ ↔ *hcp*$_2$ (Ex.)	0.74	0.72

Pathway	E_a^{for}	E_a^{rev}
ob$_0$ ↔ *ob*$_1$	0.02	0.02
ob$_0$ ↔ *ob*$_2$	0.42	0.42
ob$_0$ ↔ *ob*$_2$ (Ex.)	0.46	0.46

Pathway	E_a^{for}	E_a^{rev}
h$_0$ ↔ *h*$_1$	0.30	0.30
h$_0$ ↔ *h*$_1$ (Ex.)	0.59	0.59
h$_0$ ↔ *h*$_2$	0.42	0.42

Figure S4. Schematic representation, energy profile and PBE activation energies E_a of terrace self-diffusion processes on Mg(0001), Mg(10$\bar{1}$0), and Mg(10$\bar{1}$1). Green-colored atoms mark the initial, while red-colored atoms mark the final positions. The values are given in eV.

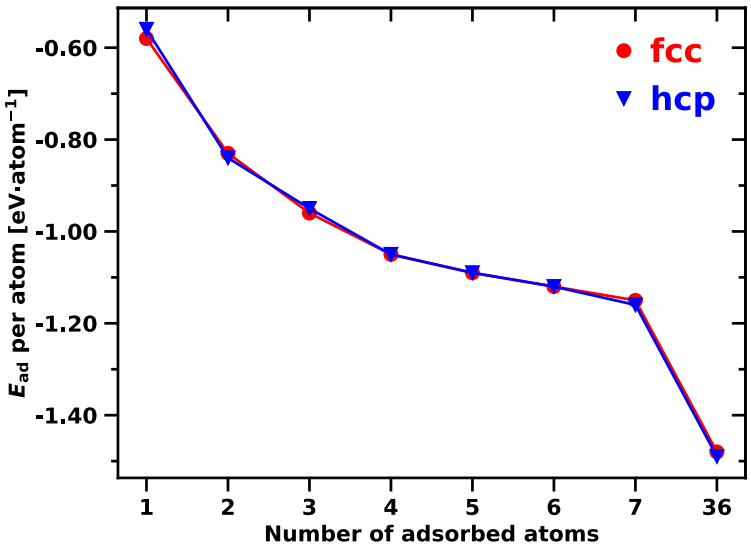

Figure S5. Adsorption energies per atom for islands of different sizes adsorbed in *fcc* and *hcp* positions on 6x6 Mg(0001). From a heptamer onwards, islands in *hcp* positions are more stable. Trimers, pentamers, and hexamers may form different conformations, with the most thermodynamically stable conformation used for the plot. 36 atoms correspond to a full monolayer.

Table S9. Adsorption energies per atoms for islands of different sizes absorbed in *fcc* and *hcp* positions on 6x6 Mg(0001). The last column shows the stacking fault energy $\Delta E_{\mathrm{ad}} = E_{\mathrm{ad},fcc} - E_{\mathrm{ad},hcp}$. Units are given in eV·atom^{-1}.

Island size	*fcc* E_{ad} per atom	*hcp* E_{ad} per atom	Stacking-fault energy ΔE_{ad}
1	-0.58	-0.56	-0.02
2	-0.83*	-0.84**	0.01
3	-0.96, -0.93	-0.95, -0.93	-0.01
4	-1.05	-1.05	0.00
5	-1.09, -1.07	-1.09. -1.07	0.00
6	-1.12, -1.10, -1.08	-1.12, -1.10, -1.09	0.00
7	-1.15	-1.16	0.01
36 (Full monolayer)	-1.48	-1.49	0.01

*** Both adsorbates are in *bridge*-like positions as shown in** Error! Reference source not found.**a.**

**** Adsorbates are in a *fcc* and a *hcp* position, respectively as shown in** Error! Reference source not found.**b.**

Table S10. Pre-exponential factors ν, activation energies E_a, rate constants $k_{@RT}$, and activation temperatures T_a for forward and backward various self-diffusion processes from PBE calculations on Mg(0001). The values are given in 10^{12} Hz, eV, Hz, and K respectively.

System	Path	Pathway	ν^{for}	E_a^{for}	$k_{@RT}^{for}$	T_a^{for}	ν^{rev}	E_a^{rev}	$k_{@RT}^{rev}$	T_a^{rev}
Dimer	Merge	$D_0 \leftrightarrow D_1$	-	0.00	-	0	-	0.49	-	194
		$D_2 \leftrightarrow D_3$	-	0.00	-	2	-	0.46	-	183
	Concerted	$CD_0 \leftrightarrow CD_1$	0.7	0.07	1.3E+11	30	2.2	0.07	4.1E+10	29
		$CD_0 \leftrightarrow CD_2$	0.4	0.01	5.4E+11	6	0.9	0.01	2.2E+11	5
Trimer	Merge	$T_0 \leftrightarrow T_1$	-	0.00	-	1	-	0.64	-	254
	Concerted	$CT_0 \leftrightarrow CT_1$	9.2	0.02	3.8E+10	7	3.8	0.12	4.5E+12	46
	Linear	$TL_0 \leftrightarrow TL_2$	2.3	0.01	1.1E+05	6	10.4	0.47	1.3E+12	180
		$TL_1 \leftrightarrow TL_2$	1.5	0.02	3.3E+04	7	2.3	0.46	7.3E+11	186
		$TL_3 \leftrightarrow TL_5$	1.5	0.00	5.3E+03	1	0.6	0.47	1.3E+12	201
		$TL_4 \leftrightarrow TL_5$	1.2	0.01	6.9E+03	3	0.6	0.46	9.1E+11	198
		$TL_6 \leftrightarrow TL_8$	0.7	0.01	1.8E+04	3	4.3	0.49	5.8E+11	194
		$TL_7 \leftrightarrow TL_8$	0.9	0.02	1.7E+04	8	4.0	0.49	4.1E+11	195
	Interchange	$TI_0 \leftrightarrow TI_1$	2.6	0.06	5.2E+10	24	39.8	0.17	2.5E+11	62
		$TI_0 \leftrightarrow TI_2$	0.4	0.07	1.3E+09	30	3.8	0.20	2.3E+10	81
Step-edge	[11$\bar{2}$0]-step	$S_0 \leftrightarrow S_1$	1.8	0.03	1.3E+09	12	19.0	0.70	1.1E+09	267
		$S_1 \leftrightarrow S_2$	6.4	0.22	1.3E+09	85	6.4	0.22	1.1E+09	85
	[$\bar{1}\bar{1}$20]-step	$S_3 \leftrightarrow S_4$	1.1	0.02	5.2E+09	7	5.5	0.63	5.2E+09	247
		$S_4 \leftrightarrow S_5$	1.9	0.15	5.2E+09	61	1.9	0.15	5.2E+09	61
Step-vacancy	[11$\bar{2}$0]-step	$SV_0 \leftrightarrow SV_1$	0.6	0.03	2.8E-07	12	19.4	1.15	2.0E+11	438
	[$\bar{1}\bar{1}$20]-step	$SV_2 \leftrightarrow SV_3$	0.4	0.02	3.9E-08	10	54.1	1.23	1.7E+11	451
Kink	[11$\bar{2}$0]-step	$K_0 \leftrightarrow K_1$	9.4	0.45	1.8E+05	174	2.8	0.17	2.9E+09	70
		$K_0 \leftrightarrow K_2$	21.4	0.91	4.1E-03	346	1.5	0.02	7.4E+11	7
		$K_0 \leftrightarrow K_3$	4.9	0.51	8.7E+03	202	3.4	0.29	3.5E+07	117
	[$\bar{1}\bar{1}$20]-step	$K_4 \leftrightarrow K_5$	8.3	0.46	8.7E+04	181	3.0	0.12	2.8E+10	48
		$K_4 \leftrightarrow K_6$	17.9	0.92	2.6E-03	350	0.4	0.01	3.2E+11	3
		$K_4 \leftrightarrow K_7$	5.4	0.56	1.1E+03	223	2.2	0.22	3.1E+08	92
Inner-corner	60° corner: [11$\bar{2}$0]-step	$IC_0 \leftrightarrow IC_1$	11.2	0.63	1.5E+02	244	4.7	0.10	9.7E+10	39
	60° corner: [$\bar{1}\bar{1}$20]-step	$IC_2 \leftrightarrow IC_3$	13.9	0.62	3.4E+02	237	4.1	0.08	2.0E+11	30
	120° corner	$IC_4 \leftrightarrow IC_5$	6.8	0.43	3.1E+05	168	5.2	0.18	3.8E+09	72
		$IC_4 \leftrightarrow IC_6$	5.6	0.43	2.1E+05	171	2.4	0.10	4.1E+10	42
Outer-corner	240° corner	$OC_0 \leftrightarrow OC_1$	0.7	0.29	1.2E+08	125	2.6	0.22	1.5E+12	88
		$OC_0 \leftrightarrow OC_1$ (Ex.)	8.6	0.41	9.3E+05	158	9.1	0.33	2.1E+07	128
	300° corner: [11$\bar{2}$0]-step	$OC_2 \leftrightarrow OC_3$ $OC_5 \leftrightarrow OC_4$	1.0	0.24	9.5E+07	99	4.0	0.00	3.5E+12	1
		$OC_3 \leftrightarrow OC_4$	1.3	0.03	3.4E+11	14	1.6	0.03	4.2E+11	14
		$OC_2 \leftrightarrow OC_5$ (Ex.)	8.0	0.32	3.1E+07	123	7.8	0.32	3.0E+07	123

	300° corner: [$\bar{1}\bar{1}$20]-step	$OC_6 \leftrightarrow OC_7$ $OC_8 \leftrightarrow OC_7$	0.2	0.20	7.2E+07	89	2.0	0.03	7.4E+11	10
		$OC_6 \leftrightarrow OC_8$ **(Ex.)**	1.5	0.16	2.7E+09	66	2.2	0.16	4.0E+09	65
Step-down	**[11$\bar{2}$0]-step**	$E_0 \leftrightarrow E_1$	2.0	0.09	1.5E+00	38	13.6	0.75	5.2E+10	289
		$E_0 \leftrightarrow E_1$ **(Ex.)**	2.4	0.01	7.0E+01	2	21.5	0.67	1.9E+12	253
	[$\bar{1}\bar{1}$20]-step	$E_2 \leftrightarrow E_3$	0.8	0.16	7.5E+00	67	8.5	0.70	1.6E+09	273
		$E_2 \leftrightarrow E_3$ **(Ex.)**	-	0.02	-	6	-	0.56	-	222
Step-down (dimer)	**[11$\bar{2}$0]-step**	$ED_0 \leftrightarrow ED_1$	6.9	0.58	2.1E+00	226	10.1	0.74	8.9E+02	286
		$ED_0 \leftrightarrow ED_1$ **(Ex.)**	4.4	0.21	2.7E+06	85	7.6	0.38	9.9E+08	147
	[$\bar{1}\bar{1}$20]-step	$ED_2 \leftrightarrow ED_3$	15.1	0.67	4.7E+00	256	2.6	0.68	4.6E+01	277
		$ED_2 \leftrightarrow ED_3$ **(Ex.)**	3.0	0.11	8.2E+09	44	3.2	0.15	4.1E+10	61
Upper-step	**[11$\bar{2}$0]-step**	$US_0 \leftrightarrow US_1$	1.7	0.02	3.1E+11	6	1.7	0.01	1.2E+12	2
		$US_1 \leftrightarrow US_2$	1.7	0.01	1.2E+12	4	0.8	0.03	3.1E+11	11
		$US_2 \leftrightarrow US_3$	0.9	0.02	4.9E+11	6	1.3	0.02	7.2E+11	6
	[$\bar{1}\bar{1}$20]-step	$US_4 \leftrightarrow US_5$	0.8	0.00	2.9E+11	1	2.9	0.03	2.1E+12	12
		$US_5 \leftrightarrow US_6$	2.2	0.00	2.1E+12	0	0.6	0.02	2.9E+11	7

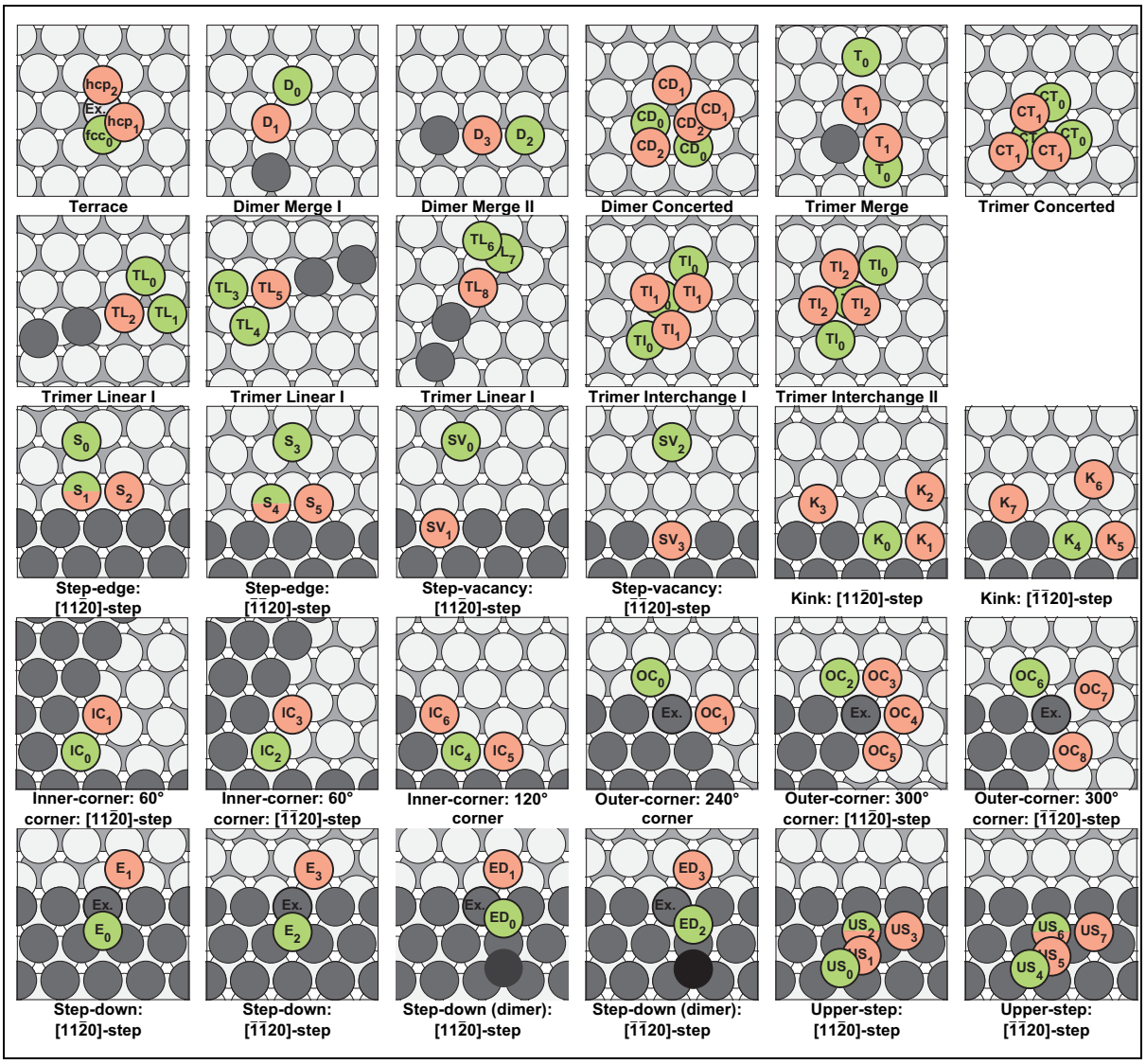

Figure S6. Schematic representation of all investigated diffusion pathways on Mg(0001).

Dimer: Merge 1

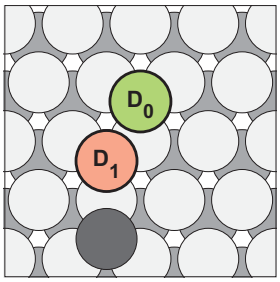

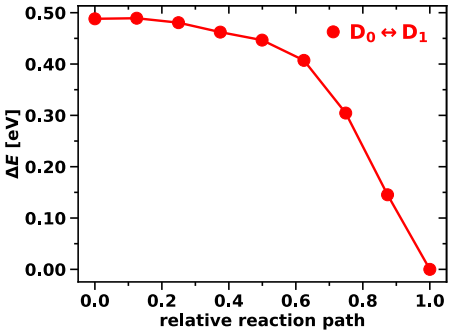

Pathway	E_a^{for}	E_a^{rev}
$D_0 \leftrightarrow D_1$	0.00	0.49

Dimer: Merge 2

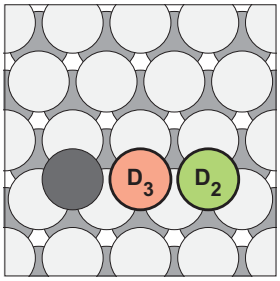

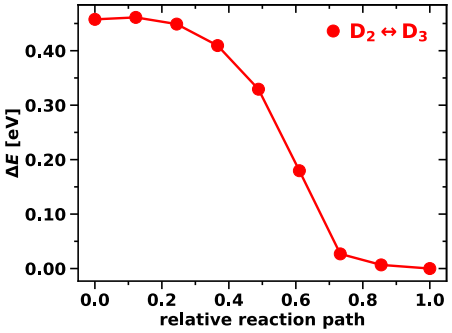

Pathway	E_a^{for}	E_a^{rev}
$D_2 \leftrightarrow D_3$	0.00	0.46

Dimer: Concerted

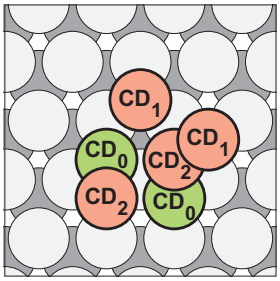

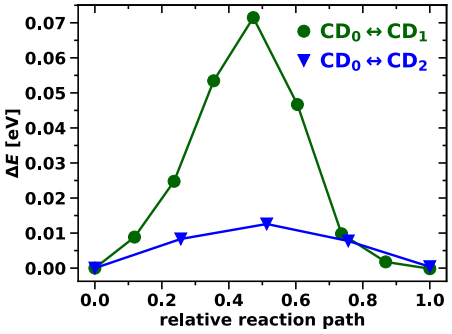

Pathway	E_a^{for}	E_a^{rev}
$CD_0 \leftrightarrow CD_1$	0.07	0.07
$CD_0 \leftrightarrow CD_2$	0.01	0.01

Trimer: Merge

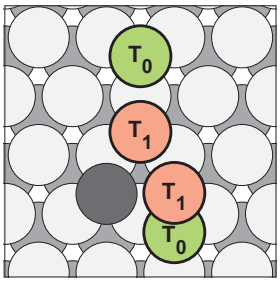

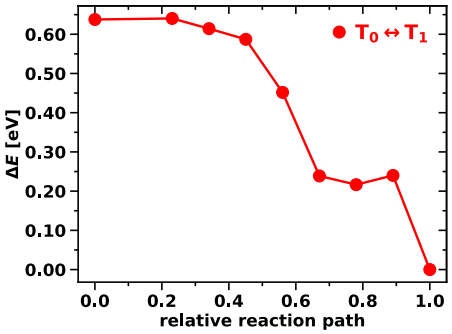

Pathway	E_a^{for}	E_a^{rev}
$T_0 \leftrightarrow T_1$	0.00	0.64

Trimer: Concerted

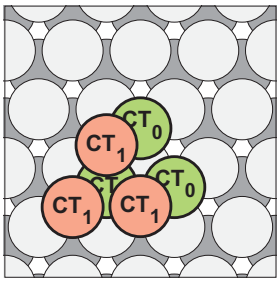

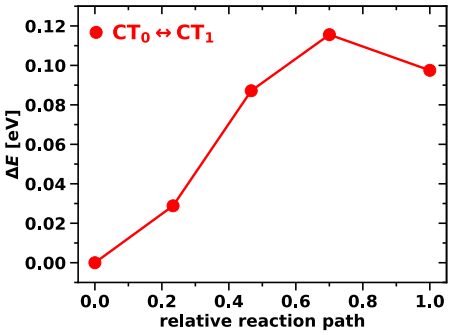

Pathway	E_a^{for}	E_a^{rev}
$CT_0 \leftrightarrow CT_1$	0.02	0.12

Trimer: Linear 1

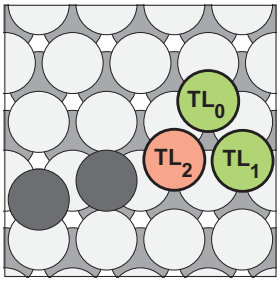

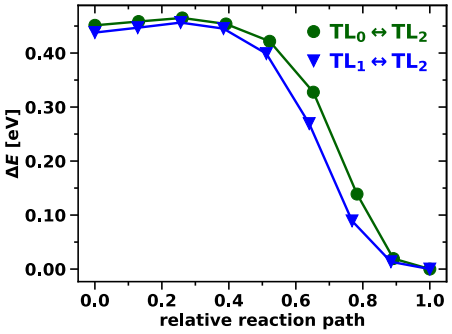

Pathway	E_a^{for}	E_a^{rev}
$TL_0 \leftrightarrow TL_2$	0.01	0.47
$TL_1 \leftrightarrow TL_2$	0.02	0.46

Trimer: Linear 2

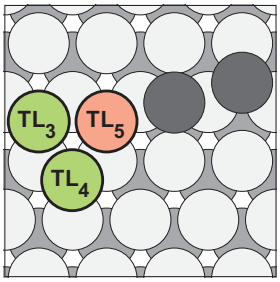

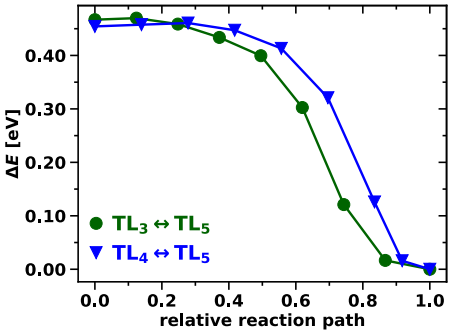

Pathway	E_a^{for}	E_a^{rev}
$TL_3 \leftrightarrow TL_5$	0.00	0.47
$TL_4 \leftrightarrow TL_5$	0.01	0.46

Trimer: Linear 3

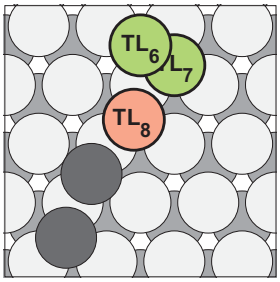

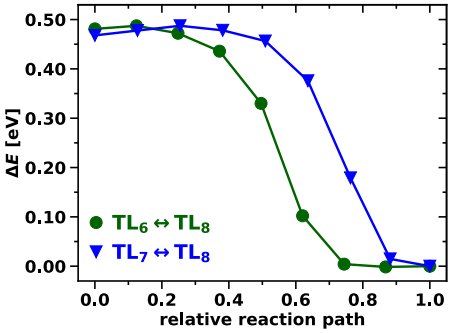

Pathway	E_a^{for}	E_a^{rev}
$TL_6 \leftrightarrow TL_8$	0.01	0.49
$TL_7 \leftrightarrow TL_8$	0.02	0.49

Trimer: Interchange 1

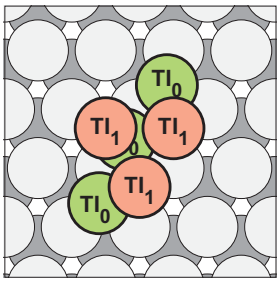

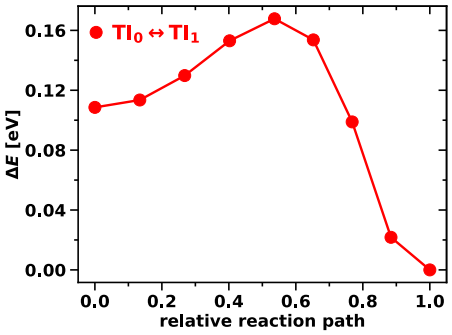

Pathway	E_a^{for}	E_a^{rev}
$Tl_0 \leftrightarrow Tl_1$	0.06	0.17

Trimer: Interchange 2

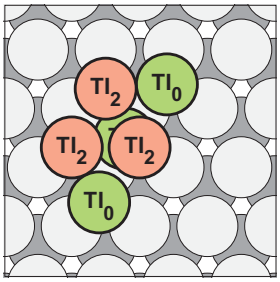

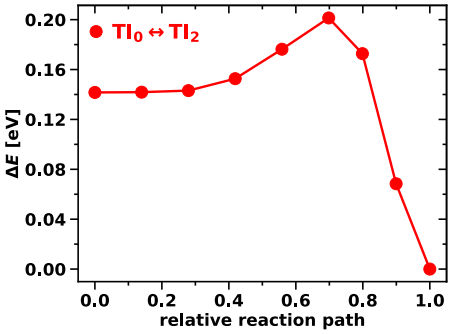

Pathway	E_a^{for}	E_a^{rev}
$Tl_0 \leftrightarrow Tl_2$	0.07	0.20

Step-edge: [11$\bar{2}$0]-step

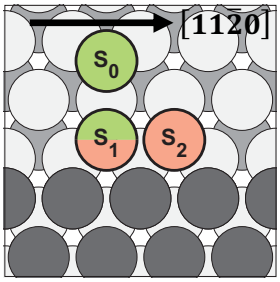

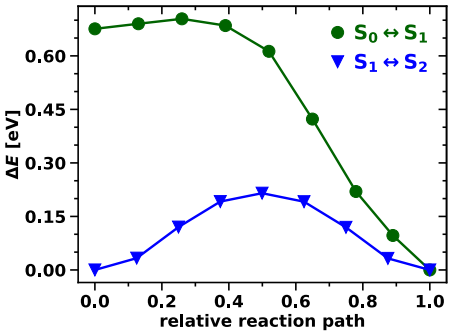

Pathway	E_a^{for}	E_a^{rev}
$S_0 \leftrightarrow S_1$	0.03	0.70
$S_1 \leftrightarrow S_2$	0.22	0.22

Step-edge: [$\bar{1}\bar{1}$20]-step

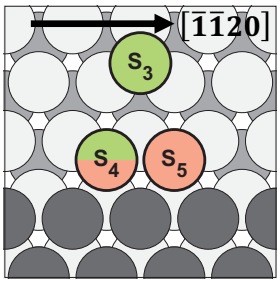

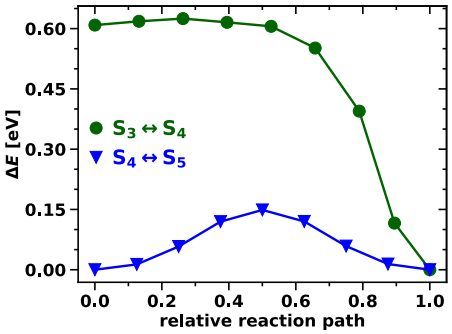

Pathway	E_a^{for}	E_a^{rev}
$S_3 \leftrightarrow S_4$	0.02	0.63
$S_4 \leftrightarrow S_5$	0.15	0.15

Step-vacancy: [11$\bar{2}$0]-step

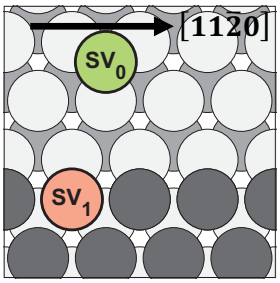

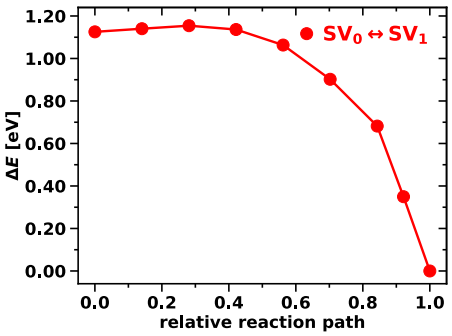

Pathway	E_a^{for}	E_a^{rev}
$SV_0 \leftrightarrow SV_1$	0.03	1.15

Step-vacancy: [$\bar{1}\bar{1}$20]-step

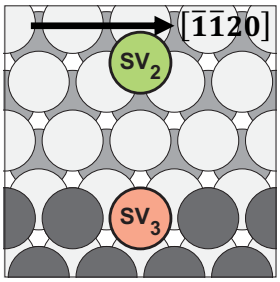

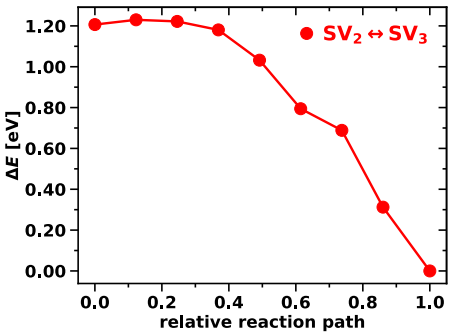

Pathway	E_a^{for}	E_a^{rev}
$SV_2 \leftrightarrow SV_3$	0.02	1.23

Kink: [11$\bar{2}$0]-step

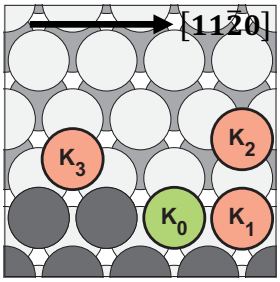

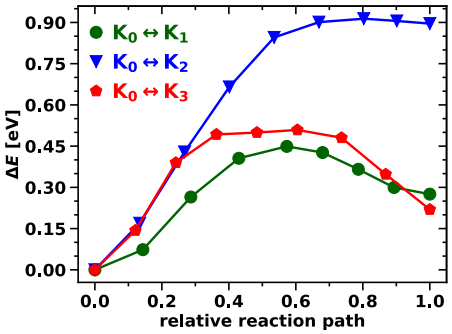

Pathway	E_a^{for}	E_a^{rev}
$K_0 \leftrightarrow K_1$	0.45	0.17
$K_0 \leftrightarrow K_2$	0.91	0.02
$K_0 \leftrightarrow K_3$	0.51	0.29

Kink: [$\bar{1}\bar{1}$20]-step

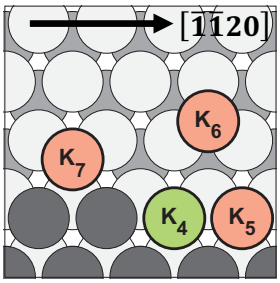

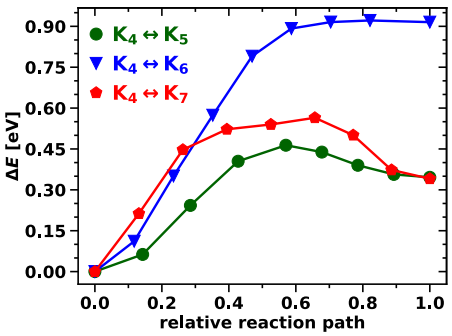

Pathway	E_a^{for}	E_a^{rev}
$K_4 \leftrightarrow K_5$	0.46	0.12
$K_4 \leftrightarrow K_6$	0.92	0.01
$K_4 \leftrightarrow K_7$	0.56	0.22

Inner-corner: 60° corner: [11$\bar{2}$0]-step

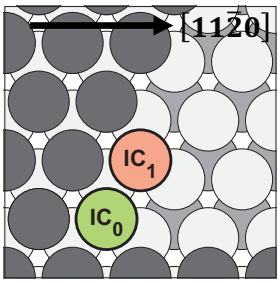

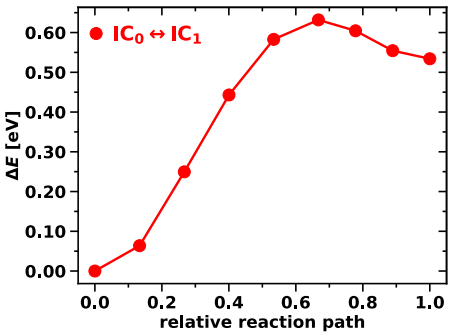

Pathway	E_a^{for}	E_a^{rev}
$IC_0 \leftrightarrow IC_1$	0.63	0.10

Inner-corner: 60° corner: [$\bar{1}\bar{1}$20]-step

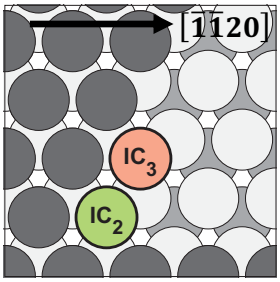

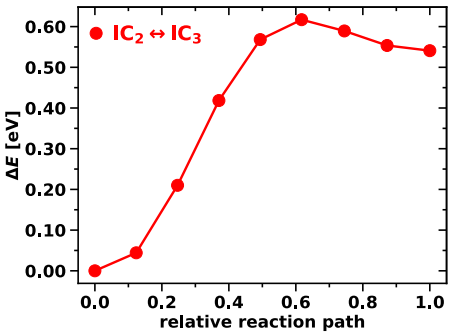

Pathway	E_a^{for}	E_a^{rev}
$IC_2 \leftrightarrow IC_3$	0.62	0.08

Inner-corner: 120° corner

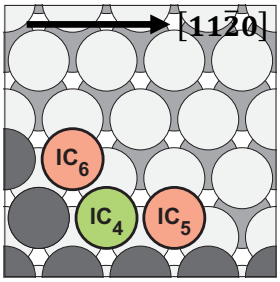

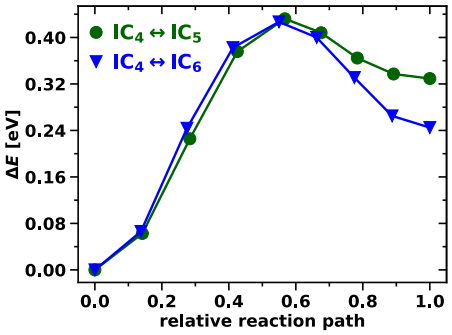

Pathway	E_a^{for}	E_a^{rev}
$IC_4 \leftrightarrow IC_5$	0.43	0.18
$IC_4 \leftrightarrow IC_6$	0.43	0.10

Outer-corner: 240° corner

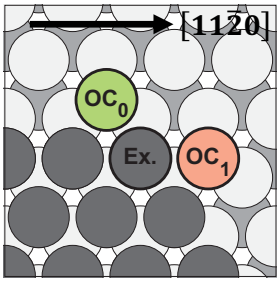

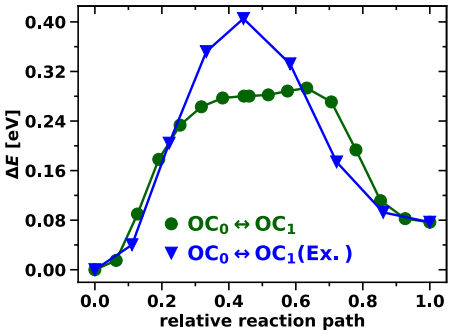

Pathway	E_a^{for}	E_a^{rev}
$OC_0 \leftrightarrow OC_1$	0.29	0.22
$OC_0 \leftrightarrow OC_1$ (Ex.)	0.41	0.33

Outer-corner: 300° corner: [11$\bar{2}$0]-step

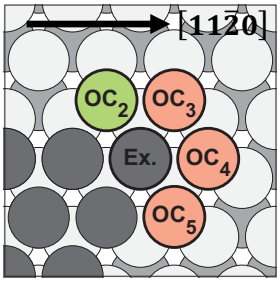

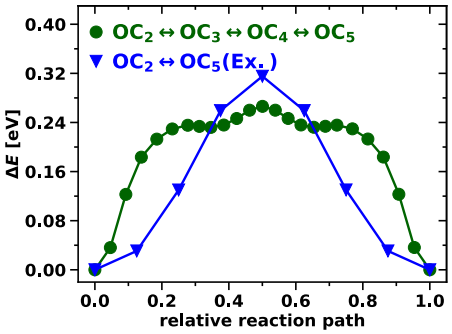

Pathway	E_a^{for}	E_a^{rev}
$OC_2 \leftrightarrow OC_3$ / $OC_5 \leftrightarrow OC_4$	0.24	0.00
$OC_3 \leftrightarrow OC_4$	0.03	0.03
$OC_2 \leftrightarrow OC_5$ (Ex.)	0.32	0.32

Outer-corner: 300° corner: [$\bar{1}\bar{1}$20]-step

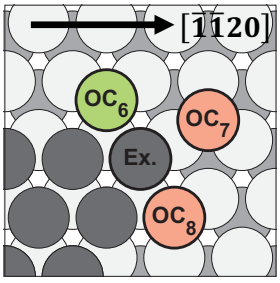

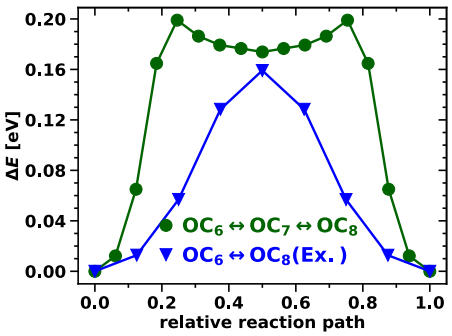

Pathway	E_a^{for}	E_a^{rev}
$OC_6 \leftrightarrow OC_7$ / $OC_8 \leftrightarrow OC_7$	0.20	0.03
$OC_6 \leftrightarrow OC_8$ (Ex.)	0.16	0.16

Step-down: [11$\bar{2}$0]-step

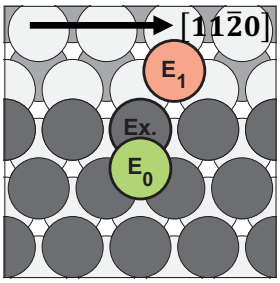

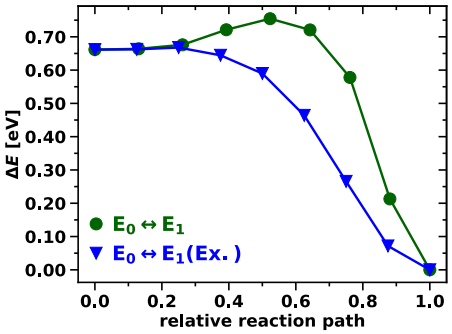

Pathway	E_a^{for}	E_a^{rev}
$E_0 \leftrightarrow E_1$	0.09	0.75
$E_0 \leftrightarrow E_1$ (Ex.)	0.01	0.67

Step-down: [$\bar{1}\bar{1}$20]-step

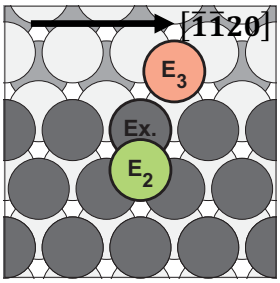

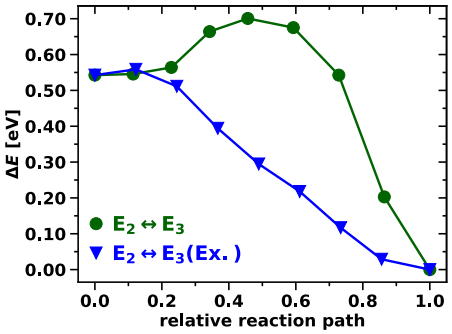

Pathway	E_a^{for}	E_a^{rev}
$E_2 \leftrightarrow E_3$	0.16	0.70
$E_2 \leftrightarrow E_3$ (Ex.)	0.02	0.56

Step-down (dimer): [11$\bar{2}$0]-step

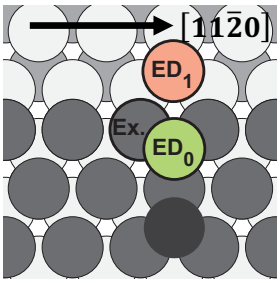

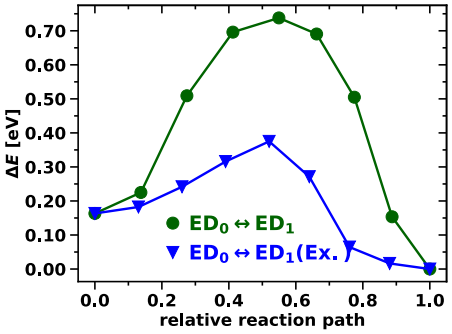

Pathway	E_a^{for}	E_a^{rev}
$ED_0 \leftrightarrow ED_1$	0.58	0.74
$ED_0 \leftrightarrow ED_1$ (Ex.)	0.21	0.38

Step-down (dimer): [$\bar{1}\bar{1}$20]-step

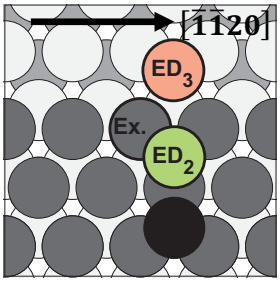

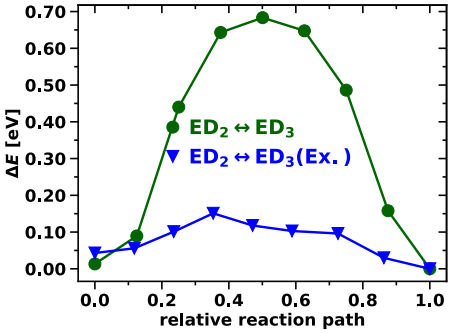

Pathway	E_a^{for}	E_a^{rev}
$ED_2 \leftrightarrow ED_3$	0.67	0.68
$ED_2 \leftrightarrow ED_3$ (Ex.)	0.11	0.15

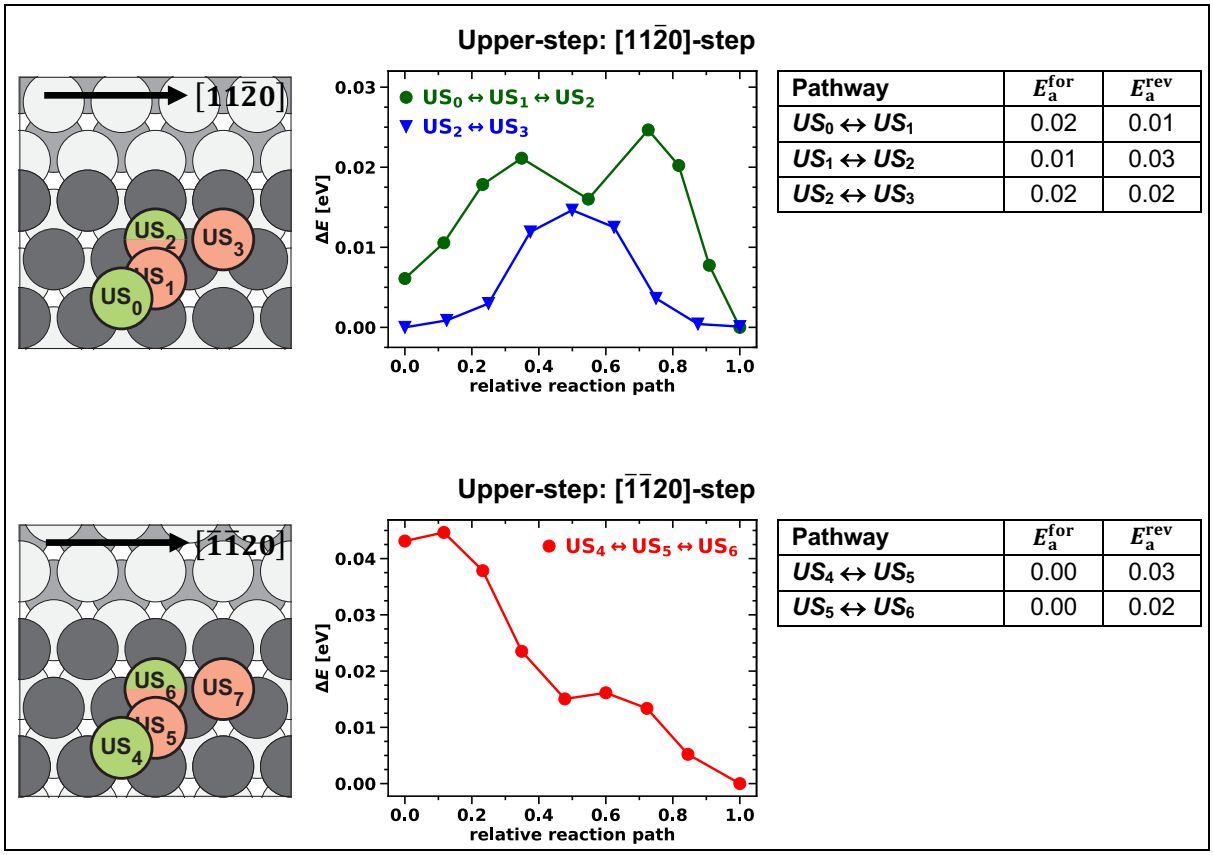

Pathway	E_a^{for}	E_a^{rev}
$US_0 \leftrightarrow US_1$	0.02	0.01
$US_1 \leftrightarrow US_2$	0.01	0.03
$US_2 \leftrightarrow US_3$	0.02	0.02

Pathway	E_a^{for}	E_a^{rev}
$US_4 \leftrightarrow US_5$	0.00	0.03
$US_5 \leftrightarrow US_6$	0.00	0.02

Figure S7. Schematic representation, energy profile and PBE activation energies E_a of self-diffusion processes studied on Mg(0001). Green-colored atoms mark the initial, while red-colored atoms mark the final positions. The values are given in eV.

Table S11. Pre-exponential factors ν, activation energies E_a, rate constants $k_{@RT}$, and activation temperatures T_a for forward and backward various self-diffusion processes from PBE calculations on Mg(10$\bar{1}$1). The values are given in 10^{12} Hertz, eV, Hz, and K, respectively.

System	Path	Pathway	ν^{for}	E_a^{for}	$k_{@RT}^{for}$	T_a^{for}	ν^{rev}	E_a^{rev}	$k_{@RT}^{rev}$	T_a^{rev}
Dimer	Merge	$d_0 \leftrightarrow d_1$	11.6	0.25	5.0E+08	98	23.6	0.58	2.6E+03	218
		$d_2 \leftrightarrow d_3$	4.8	0.19	2.8E+09	75	2.6	0.13	1.5E+10	53
		$d_3 \leftrightarrow d_1$	2.4	0.15	6.0E+09	61	10.6	0.51	2.0E+04	197
		$d_4 \leftrightarrow d_1$	10.2	0.37	5.2E+06	142	11.9	0.67	3.2E+01	259
	Concerted	$cd_0 \leftrightarrow cd_1$	19.0	0.54	1.0E+04	205	18.9	0.54	1.0E+04	205
Trimer	Merge	$t_0 \leftrightarrow t_1$	5.6	0.26	2.3E+08	103	13.1	0.58	1.2E+03	223
		$t_2 \leftrightarrow t_3$	7.8	0.19	4.6E+09	73	4.1	0.20	1.3E+09	82
		$t_3 \leftrightarrow t_1$	3.3	0.27	7.6E+07	109	11.0	0.54	5.7E+03	209
		$t_4 \leftrightarrow t_5$	8.1	0.31	3.5E+07	122	6.3	0.57	9.3E+02	225
		$t_5 \leftrightarrow t_1$	1.6	0.24	1.4E+08	98	4.9	0.28	8.4E+07	110
Step-edge	[$\bar{1}2\bar{1}0$]A-step	$s_0 \leftrightarrow s_1$	9.6	0.35	1.1E+07	134	9.9	0.59	6.8E+02	229
		$s_1 \leftrightarrow s_2$	2.7	0.13	1.8E+10	51	4.1	0.13	2.8E+10	50
	[$\bar{1}2\bar{1}0$]B-step	$s_3 \leftrightarrow s_4$	9.3	0.44	2.6E+05	171	6.8	0.73	2.3E+00	285
		$s_4 \leftrightarrow s_5$	3.7	0.16	8.0E+09	62	3.4	0.16	7.3E+09	62
	[$1\bar{2}10$]A-step	$s_6 \leftrightarrow s_7$	6.8	0.14	2.5E+10	56	0.1	0.18	1.1E+08	81
		$s_7 \leftrightarrow s_8$	1.0	0.01	6.3E+11	5	0.6	0.01	4.1E+11	5
	[$1\bar{2}10$]B-step	$s_9 \leftrightarrow s_{10}$	4.5	0.36	2.7E+06	144	15.6	0.95	7.5E-04	363
		$s_{10} \leftrightarrow s_{11}$	10.2	0.40	1.2E+06	156	11.3	0.40	1.3E+06	156
	[$10\bar{1}2$]-step	$s_{12} \leftrightarrow s_{13}$	18.5	0.18	1.5E+10	68	46.2	0.71	3.4E+01	260
		$s_{13} \leftrightarrow s_{14}$	6.8	0.45	1.3E+05	177	7.4	0.45	1.3E+05	176
Step-down	[$\bar{1}2\bar{1}0$]A-step	$e_0 \leftrightarrow e_1$	10.2	0.44	3.1E+05	169	10.3	0.67	3.8E+01	258
		$e_0 \leftrightarrow e_2$ (Ex.)	4.1	0.11	5.5E+10	44	3.9	0.34	6.0E+06	135
	[$\bar{1}2\bar{1}0$]B-step	$e_3 \leftrightarrow e_4$	8.3	0.43	3.3E+05	168	13.7	0.75	1.7E+00	288
		$e_3 \leftrightarrow e_4$ (Ex.)	5.4	0.26	1.8E+08	103	7.2	0.58	7.1E+02	228
	[$1\bar{2}10$]A-step	$e_5 \leftrightarrow e_6$	6.0	0.29	7.3E+07	113	2.4	0.04	4.9E+11	16
		$e_6 \leftrightarrow e_7$	3.5	0.12	3.3E+10	47	1.3	0.42	7.8E+04	175
		$e_5 \leftrightarrow e_7$ (Ex.)	9.9	0.47	8.6E+04	182	1.6	0.53	1.5E+03	217
	[$1\bar{2}10$]B-step	$e_8 \leftrightarrow e_9$	6.9	0.44	1.7E+05	174	11.0	0.96	3.6E-04	371
		$e_8 \leftrightarrow e_{10}$ (Ex.)	3.3	0.07	1.9E+11	29	8.4	0.59	6.5E+02	229
	[$10\bar{1}2$]-step	$e_{11} \leftrightarrow e_{12}$	18.7	0.38	5.5E+06	144	21.6	0.89	1.2E-02	336
		$e_{11} \leftrightarrow e_{12}$ (Ex.)	6.8	0.20	2.8E+09	77	12.5	0.71	9.4E+00	271

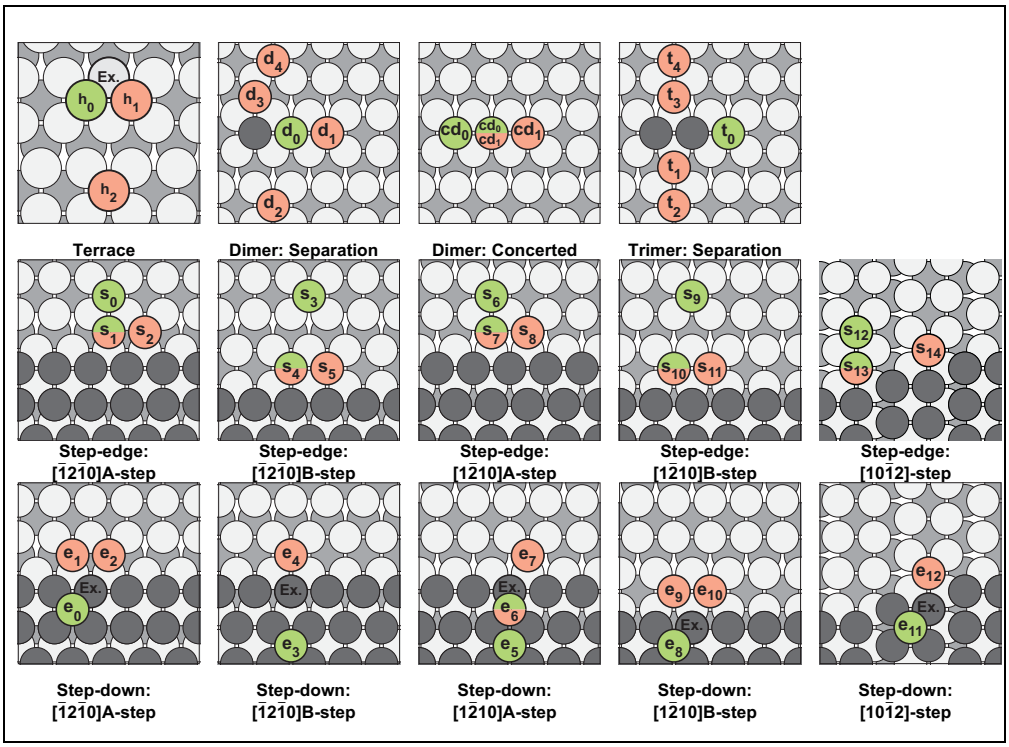

Figure S8. Schematic representation of all investigated diffusion pathways on Mg(10$\bar{1}$1).

Dimer: Merge

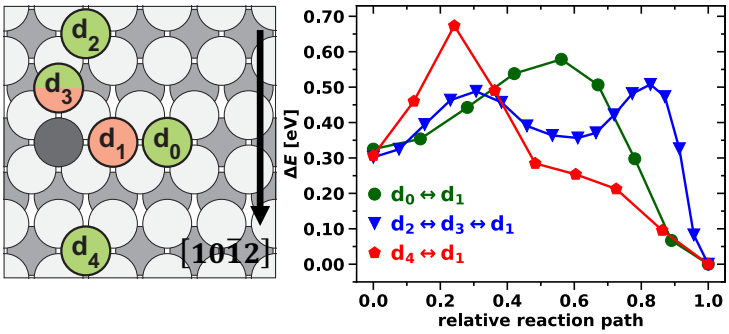

Pathway	E_a^{for}	E_a^{rev}
$d_0 \leftrightarrow d_1$	0.25	0.58
$d_2 \leftrightarrow d_3$	0.19	0.13
$d_3 \leftrightarrow d_1$	0.15	0.51
$d_4 \leftrightarrow d_1$	0.37	0.67

Dimer: Concerted

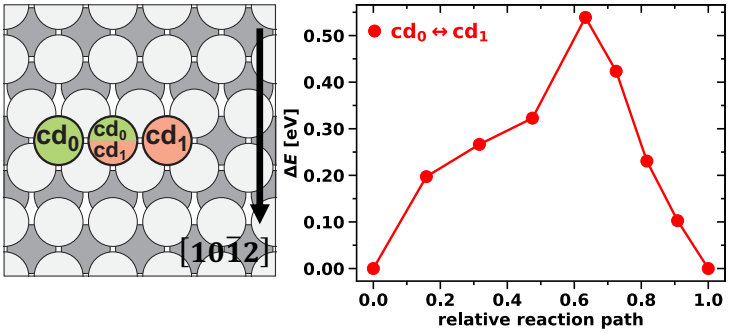

Pathway	E_a^{for}	E_a^{rev}
$cd_0 \leftrightarrow cd_1$	0.54	0.54

Trimer: Merge

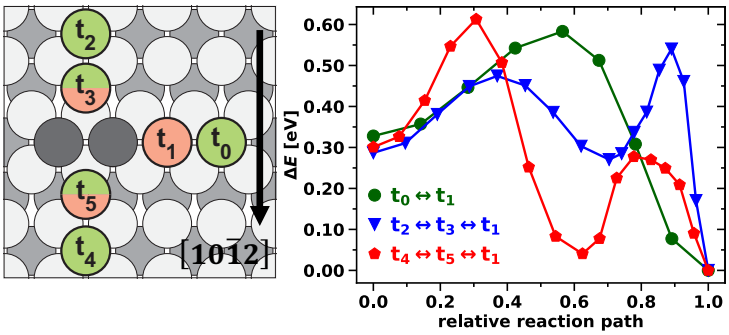

Pathway	E_a^{for}	E_a^{rev}
$t_0 \leftrightarrow t_1$	0.26	0.58
$t_2 \leftrightarrow t_3$	0.19	0.20
$t_3 \leftrightarrow t_1$	0.27	0.54
$t_4 \leftrightarrow t_5$	0.31	0.57
$t_5 \leftrightarrow t_1$	0.24	0.28

Step-edge: [$\bar{1}2\bar{1}0$]A-step

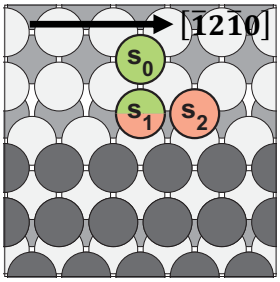

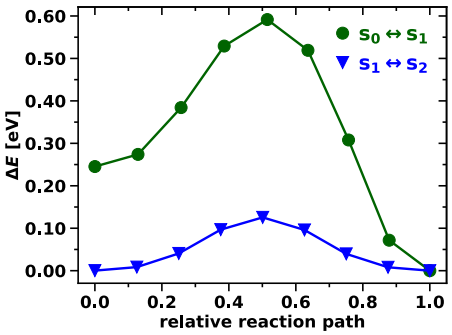

Pathway	E_a^{for}	E_a^{rev}
$s_0 \leftrightarrow s_1$	0.35	0.59
$s_1 \leftrightarrow s_2$	0.13	0.13

Step-edge: [$\bar{1}2\bar{1}0$]B-step

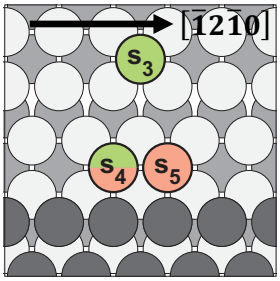

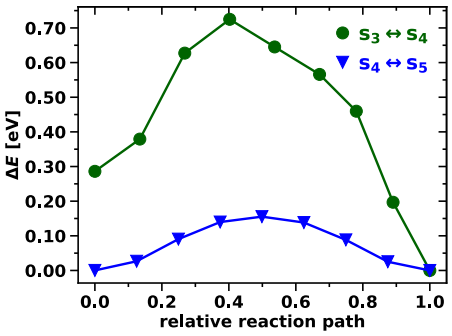

Pathway	E_a^{for}	E_a^{rev}
$s_3 \leftrightarrow s_4$	0.44	0.73
$s_4 \leftrightarrow s_5$	0.16	0.16

Step-edge: [$1\bar{2}10$]A-step

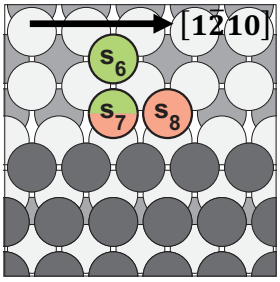

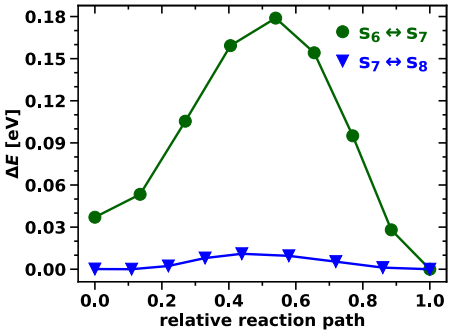

Pathway	E_a^{for}	E_a^{rev}
$s_6 \leftrightarrow s_7$	0.14	0.18
$s_7 \leftrightarrow s_8$	0.01	0.01

Step-edge: [$1\bar{2}10$]B-step

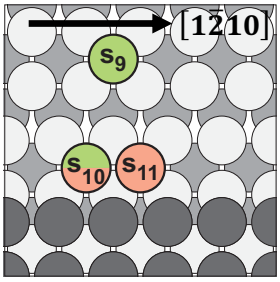

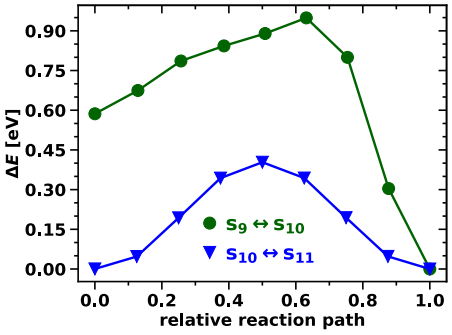

Pathway	E_a^{for}	E_a^{rev}
$s_9 \leftrightarrow s_{10}$	0.36	0.95
$s_{10} \leftrightarrow s_{11}$	0.40	0.40

Step-edge: [10$\bar{1}$2]-step

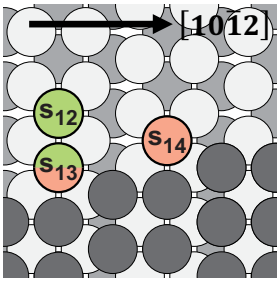

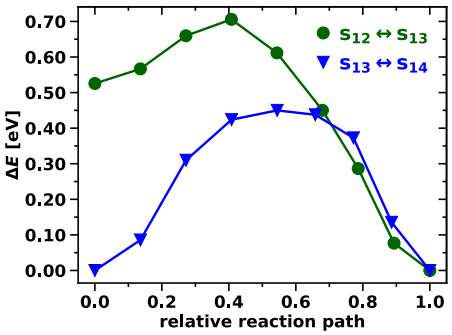

Pathway	E_a^{for}	E_a^{rev}
$s_{12} \leftrightarrow s_{13}$	0.18	0.71
$s_{13} \leftrightarrow s_{14}$	0.45	0.45

Step-down: [$\bar{1}$2$\bar{1}$0]A-step

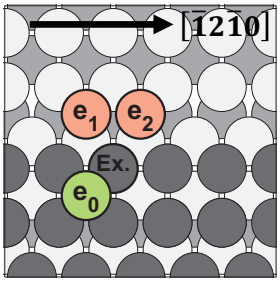

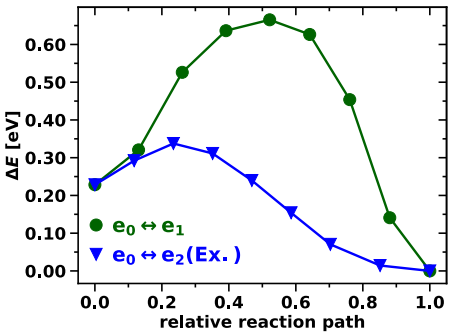

Pathway	E_a^{for}	E_a^{rev}
$e_0 \leftrightarrow e_1$	0.44	0.67
$e_0 \leftrightarrow e_2$ (Ex.)	0.11	0.34

Step-down: [$\bar{1}$2$\bar{1}$0]B-step

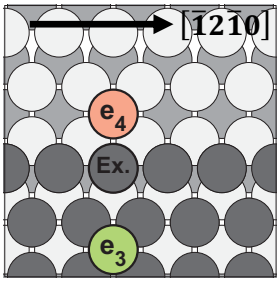

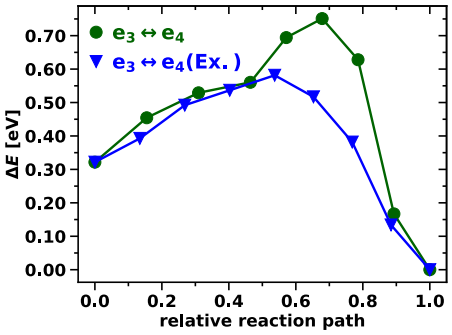

Pathway	E_a^{for}	E_a^{rev}
$e_3 \leftrightarrow e_4$	0.43	0.75
$e_3 \leftrightarrow e_4$ (Ex.)	0.26	0.58

Step-down: [1$\bar{2}$10]A-step

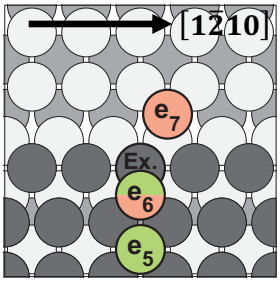

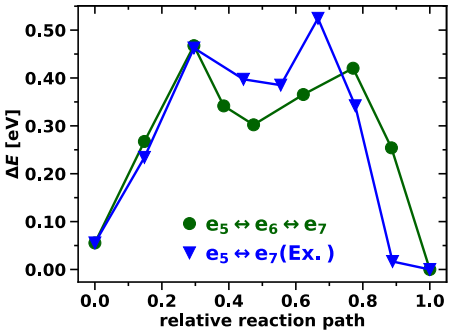

Pathway	E_a^{for}	E_a^{rev}
$e_5 \leftrightarrow e_6$	0.29	0.04
$e_6 \leftrightarrow e_7$	0.12	0.42
$e_5 \leftrightarrow e_7$ (Ex.)	0.47	0.53

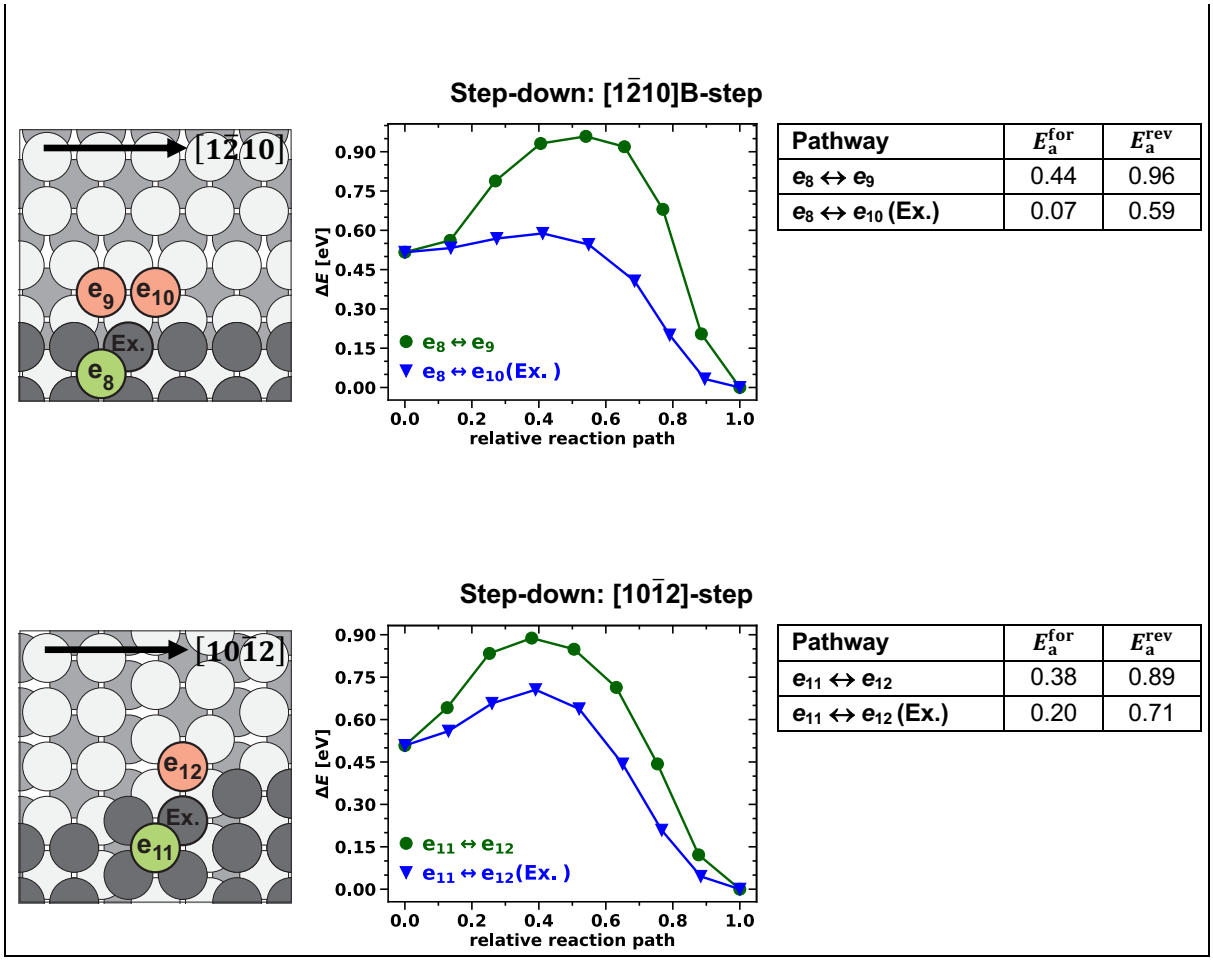

Pathway	E_a^{for}	E_a^{rev}
$e_8 \leftrightarrow e_9$	0.44	0.96
$e_8 \leftrightarrow e_{10}$ (Ex.)	0.07	0.59

Pathway	E_a^{for}	E_a^{rev}
$e_{11} \leftrightarrow e_{12}$	0.38	0.89
$e_{11} \leftrightarrow e_{12}$ (Ex.)	0.20	0.71

Figure S9. Schematic representation, energy profile and PBE activation energies E_a of self-diffusion processes studied on Mg(10$\bar{1}$1). Green-colored atoms mark the initial, while red-colored atoms mark the final positions. The values are given in eV.

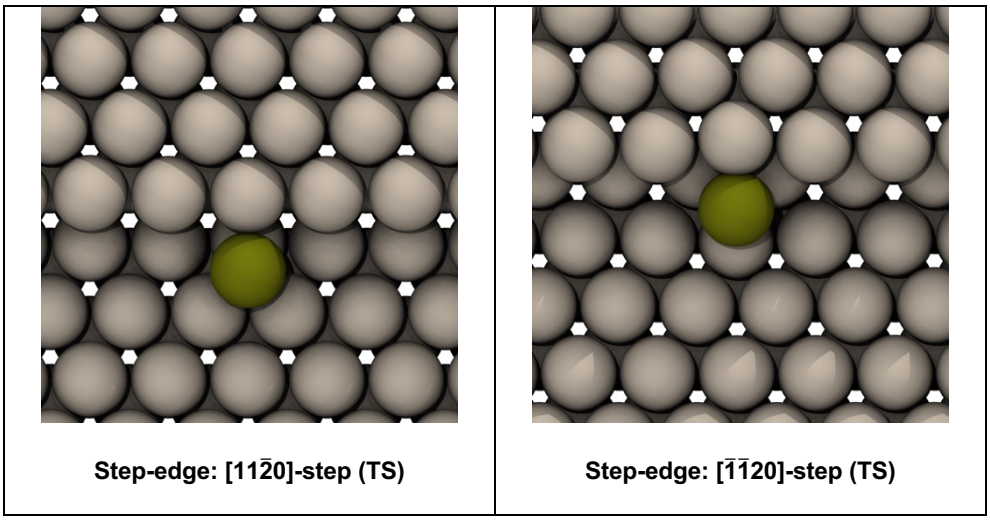

Figure S10. Transition states of step-edge diffusion pathways along [11$\bar{2}$0]- and [$\bar{1}\bar{1}$20]-steps steps. In the TS of the [$\bar{1}\bar{1}$20]-step, the nearest neighbor atom in the edge row pulls slightly back, leaving a pocket for the diffusing atom (green) to settle in a stabilized *fcc*-like position.

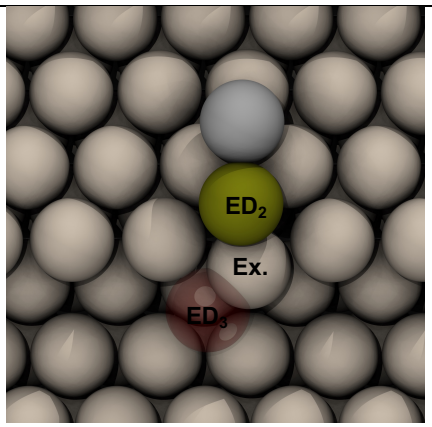

Step-down (dimer): [$\bar{1}\bar{1}$20]-step (TS)

Figure S11. Transition state of step-down (dimer) diffusion pathway along the [$\bar{1}\bar{1}$20]-step. The second atom (gray) follows the diffusing atom (green) into the *fcc* position above the exchange atom. This maintains the dimer conformation until beyond the TS and lowers the activation energy of the process.

References

[1] J. A. Moriarty, A. K. McMahan, *Phys. Rev. Lett.* **1982**, *48*, 809–812.

[2] A. K. McMahan, J. A. Moriarty, *Phys. Rev. B* **1983**, *27*, 3235–3251.

[3] J. A. Moriarty, J. D. Althoff, Phys. Rev. B **1995**, *51*, 5609–5616.

[4] H. Olijnyk, W. B. Holzapfel, *Phys. Rev. B* **1985**, *31*, 4682–4683.

[5] D. Errandonea, Y. Meng, D. Husermann, T. Uchida, *J. Phys.: Condens. Matter* **2003**, *15*, 1277–1289.

[6] G. W. Stinton, S. G. MacLeod, H. Cynn, D. Errandonea, W. J. Evans, J. E. Proctor, Y. Meng, M. I. McMahon, *Phys. Rev. B* **2014**, *90*, 134105.

[7] C. Kittel, *Introduction to Solid State Physics*, *8th ed.*, John Wiley & Sons, New York, **2004**.

[8] A. B. Alchagirov, J. P. Perdew, J. C. Boettger, R. C. Albers, C. Fiolhais, *Phys. Rev. B* **2001**, *63*, 224115.

[9] A. Kopač Lautar, D. Kopač, T. Rejec, T. Bančič, R. Dominko, *Phys. Chem. Chem. Phys.* **2019**, *21*, 2434–2442.

[10] M. Jäckle, A. Groß, *J. Chem. Phys.* **2014**, *141*, 174710.

[11] D. Stottmeister, A. Groß, *ChemSusChem* **2020**, *13*, 3147–3153.

[12] M. Alcántara Ortigoza, M. Aminpour, T. S. Rahman, *Surf. Sci.* **2015**, *632*, 14–19.

[13] E. Wachowicz, A. Kiejna, *J. Phys.: Condens. Matter* **2001**, *13*, 10767–10776.

[14] D. P. Ji, Q. Zhu, S. Q. Wang, *Surf. Sci.* **2016**, *651*, 137–146.

[15] J.-J. Tang, X.-B. Yang, L. OuYang, M. Zhu, Y.-J. Zhao, *J. Phys. D: Appl. Phys.* **2014**, *47*, 115305.

[16] I. T. Røe, S. M. Selbach, S. K. Schnell, *J. Phys. Chem. Lett.* **2020**, 2891–2895.

[17] A. B. Alchagirov, J. P. Perdew, J. C. Boettger, R. C. Albers, C. Fiolhais, *Phys. Rev. B* **2003**, *67*, 026103.

[18] R. Tran, Z. Xu, B. Radhakrishnan, D. Winston, W. Sun, K. A. Persson, S. P. Ong, *Sci. Data* **2016**, *3*, 160080.

[19] C. G. Johansen, H. Huang, T. M. Lu, *Comput. Mater. Sci.* **2009**, *47*, 121–127.

[20] B. J. Keene, *Int. Mater. Rev.* **1993**, *38*, 157–192.

[21] X.-Y. Liu, J. B. Adams, F. Ercolessi, J. A. Moriarty, *Modell. Simul. Mater. Sci. Eng.* **1996**, *4*, 293–303.

[22] D. Y. Sun, M. I. Mendelev, C. A. Becker, K. Kudin, T. Haxhimali, M. Asta, J. J. Hoyt, A. Karma, D. J. Srolovitz, *Phys. Rev. B* **2006**, *73*, 024116.

[23] M. Alcántara Ortigoza, M. Aminpour, T. S. Rahman, *Phys. Rev. B* **2015**, *91*, 115401.